Isotopic Abundance Ratios of C and O in the Dark Cloud L1521E

Jay Motka,[1] Jacob Magnusson,[1] Maya Mancini,[1] and Akash Satpathy[1]

[1] *Department of Astronomy and Steward Observatory, University of Arizona, Tucson, AZ 85721, USA*

ABSTRACT

Isotopic ratios of various elements from molecular clouds give us valuable information on the chemical and physical processes that govern astronomical processes, such as star formation. In this paper, we measure the isotopic abundance ratios of carbon and oxygen in a young, starless cloud, Lynds 1521E, by observing the line emissions of $J = 2 - 1$ rotational transition in CO and its isotopes using the Submillimeter Telescope (SMT). We use CHAOS, a powerful python package, to perform data reduction and data analysis on the observed spectra of the isotopes of CO in L1521E. The measured ratios, $\frac{^{12}C}{^{13}C}$, $\frac{^{16}O}{^{17}O}$, and $\frac{^{16}O}{^{18}O}$, are 39.95 ± 7.89, 176.57 ± 92.57, and 71.81 ± 14.22, respectively.

Keywords: isotopic ratios, starless core, abundance

1. INTRODUCTION

Different isotopic ratios inside molecular clouds give us an insight into the galactic chemical structure and evolution. The elements such as carbon and oxygen are created during stellar nucleosynthesis. Thus, the isotopic abundance ratios of these elements provide valuable information about the physics and chemistry of star formation (Langer & Penzias 1993).

To measure the isotopic abundance ratios of carbon and oxygen, carbon-based molecules such as carbon monoxide and its isotopic species are very useful. The spectra of CO and its isotopic species, ^{12}C^{17}O, ^{12}C^{18}O, ^{13}C^{16}O, ^{13}C^{17}O, and ^{13}C^{18}O, are easier to obtain from a single object as the frequencies of their $J = 2 - 1$ rotational transitions are not so far apart. Thus, it is possible to simultaneously measure two lines at a time as stated in Section 2.

The chemical compounds of starless and gravitationally bound pre-stellar cores, sometimes also known as dark clouds or dark cores, are substantially informational in understanding the initial physical conditions and chemical structures of the star formation. Thus, we look at the isotopic abundance ratios of CO and its isotopologues in a starless core situated in Taurus, Lynds 1521E (L1521E).

2. OBSERVATIONS AND DATA ANALYSIS

We used the Submillimeter Telescope (SMT), located at Mt. Graham, with a 10-meter diameter for this observation. The front end used was a 1.3 mm receiver, which can observe ALMA Band 6 (205-280 GHz). The

Corresponding author: Jay Motka
jaymotka@arizona.edu

Table 1. The information on scans and the total integration time for each line. The first section shows the information from the observation on March 06, 2021. The last two lines are for the new observation on March 07, 2021. These new observations with no contamination were used in our calculations.

Line ($J = 2 - 1$)	Rest Frequency (GHz)	No. of Scans	Total Integration Time (Seconds)
$^{12}C^{16}O$	230.53800000	18	6480
$^{13}C^{16}O$	220.39861950	18	6480
$^{12}C^{17}O$	224.71418700	24	8640
$^{13}C^{17}O$	214.57387300	24	8640
$^{12}C^{18}O$	219.56035410	24	8640
$^{13}C^{18}O$	209.41909830	24	8640
$^{12}C^{16}O$	230.53800000	4	1440
$^{13}C^{16}O$	220.39861950	2	1440

back end was 4 IF mode with 32 MHz bandwidth and 250 kHz resolution. These pieces of equipment were the most suitable as the $J = 2 - 1$ transition frequencies of the isotopologues of CO varies in between 209 GHz to 231 GHz, as shown in Table 1.

Given the combination of mixer and amplifier, the sky frequency (ν_{sky}) is determined through a chosen local oscillator frequency (ν_{LO}) and intermediate frequency (ν_{IF}), according to the formula

$$\nu_{sky} = \nu_{LO} \pm \nu_{IF}. \tag{1}$$

At SMT, the intermediate frequency range is ν_{IF} = 4-8 GHz. Thus, Equation 1 implies that we can observe 4-8 GHz above and below the chosen LO frequency. As such, we chose three different LO frequencies such that we could observe the pairs of $^{12}C^{16}O$ and $^{13}C^{16}O$ lines, $^{12}C^{17}O$ and $^{13}C^{17}O$ lines, and $^{12}C^{18}O$ and $^{13}C^{18}O$ lines simultaneously.

The observing mode used was beam switching with the beam throw of ± 2 arcmins and switching rate of 2.5 Hz. In the beam switching mode, the equipment switches between the source and background within the given beam throw at the given switching rate. In doing so, the background noise is subtracted from the source intensity at each switching cycle.

Given an expected line amplitude (T_A), the signal to noise ratio is T_A/σ_T. Here, σ_T is defined as

$$\sigma_T = \sqrt{\frac{2}{\tau\Delta\nu}} T_{sys}, \tag{2}$$

where T_{sys} is the system temperature, $\Delta\nu$ is the bandwidth, and τ is the integration time. The 1.3 mm receiver at SMT has about typical system temperature of 200-275 K at about 230GHz. Given that there are 4 samples per scan, we calculated the integration time of 90 seconds per sample to get an approximate good signal-to-noise ratios for each line using Equation 2.

L1521E has the J2000.0 coordinates (RA, Dec) of (04:29:21.0, 26:14:19.0) and a velocity of about 6.8 LSR (Local Standard of Rest). Given these coordinates, we used some programming to determine the best possible

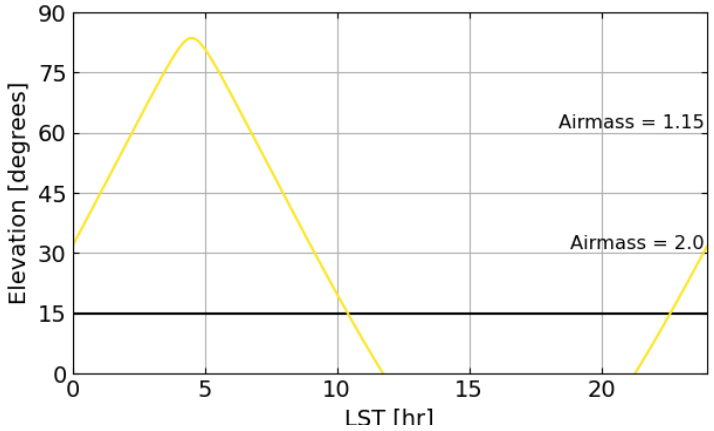

Figure 1. Elevation of L1521E as a function of LST.

time to start the observation. The observation was done from 3 LST to 9 LST on March 06, 2021. See the elevation of L1521E as a function of LST in Figure 1.

Calibration is usually done by looking at a bright continuum source to get the right aiming. As such, we started the observation by calibrating with Mars as a reference and then started observing the $J = 2 - 1$ transition lines of CO and its isotopic species in L1521E. The total integration time for each line is given in Table 1.

During the observation of $^{12}C^{16}O$ and $^{13}C^{16}O$ lines, we observed an absorption line right next to the emission line in each scan of $^{12}C^{16}O$ line emission.Thus, we could not take the correct scans of these lines. Upon further investigation, we concluded that this error occurred since we could not find an off-position without any emission in the $^{12}C^{16}O$ line during the beam switching. Thus, we also subtracted the line emission from the off-position when subtracting the noise, which resulted in contamination. Following the same observing procedure, we took some new scans of $^{12}C^{16}O$ and $^{13}C^{16}O$ lines without contamination on March 07, 2021, at about 1 LST, given a new off-position. The information containing these new scans is shown in Table 1. We used these new scans with no contamination for our calculations regarding $^{12}C^{16}O$ and $^{13}C^{16}O$ lines.

To perform data reduction and analyze the data, we utilized a python package called CHAOS (Computations for Heterodyne Analysis, Observations, and Science), designed as a python-based alternative to legacy single-dish data reduction software such as CLASS. CHAOS is designed to allow easy python scripting of customizable data reduction pipelines.

We first converted the x-axis of spectra from frequency units to velocity units using the Doppler effect according to

$$v = c\,\frac{\nu_0 - \nu}{\nu_0},$$

where ν_0 is the rest frequency, ν is the observed frequency due to the Doppler effect for motion at the velocity v. Then, we set up masks on the scans of each line according to the respective velocity range shown in Table 2.

Table 2. The integrated temperatures and the signal-to-noise ratios given the velocity range of integration and masks for each line emission from L1521E.

Line ($J = 2 - 1$)	Δv (Km/s)	$\int_{\Delta v} T_R\, dv$ K km/s	SNR
$^{12}C^{16}O$	-2.5 to 1.5	6.0332 ±0.0346	174.365
$^{13}C^{16}O$	-1.4 to 1.4	2.0895 ±0.0288	072.478
$^{12}C^{17}O$	-2.2 to 1.5	0.3632 ±0.0071	051.277
$^{13}C^{17}O$	-2.0 to 1.5	0.0148 ±0.0078	001.908
$^{12}C^{18}O$	-1.0 to 0.7	0.7058 ±0.0045	158.150
$^{13}C^{18}O$	-1.5 to 1.5	0.0312 ±0.0062	005.063

After setting the masks over the specific velocity range as not to lose any data on the line emission, we removed the noise from the rest of the spectra using the baseline fit of a polynomial of the degree of 5. We completed the data reduction for each scan of the specific lines. We then combined these scans according to the weights of the system temperature during each scan. The scans are weighted according to their system temperature, as the noise is proportional to the system temperature, as stated in Equation 2. These combined spectra of each line and velocity masks are shown in Figure 2.

Finally, we calculated the integration of temperature over the velocity range shown in Table 2 along with the signal-to-noise ratio. The results of this analysis are shown in Table 2.

3. THEORY

As stated in Mangum & Shirley (2015), we first wrote the radiative transfer equation in a form that involves the observable source radiation temperature, T_R, derived from a differencing measurement,

$$T_R = (J_\nu(T_{ex}) - J_\nu(T_{cmb}))(1 - e^{-\tau_\nu}). \quad (3)$$

Here, $J_v(T)$ is the Rayleigh-Jeans equivalent temperature, which is the equivalent temperature of a black body at the temperature T. T_{ex} is the extinction temperature, T_{CMB} is the CMB temperature, and τ_v is the optical depth.

We assumed that the optical depth is very small for all molecules. However, this assumption is not valid for $^{12}C^{16}O$. As such, we did not use $^{12}C^{16}O$ line in calculating the isotopic abundance ratios using this calculation method. Using Equation 3, for two different lines, the integrated temperature ratio became

$$\frac{\int T_{R,1}\, dv_1}{\int T_{R,2\, dv2}} = \frac{\int (J_1(T_{ex}) - J_1(T_{cmb}))\tau_1 dv_1}{\int (J_2(T_{ex}) - J_2(T_{cmb}))\tau_2 dv_2}.$$

We assumed that the temperature difference does not vary much over our spectral range. Thus, we eliminated those terms from the numerator and denominator. This left us with

$$\frac{\int T_{R,1} dv_1}{\int T_{R,2} dv_2} = \frac{\tau_1 \Delta v_1}{\tau_2 \Delta v_2}.$$

We took the optical depth to be some cross-section times the column density, which lead to

$$\frac{\tau_1}{\tau_2} = \frac{N_1 \sigma_1}{N_2 \sigma_2}.$$

Because the frequency difference between these emission lines are small, we approximated the cross section for each molecule at their respective wavelength for the $J = 2 - 1$ transition to be equal, eliminating the cross-sections.

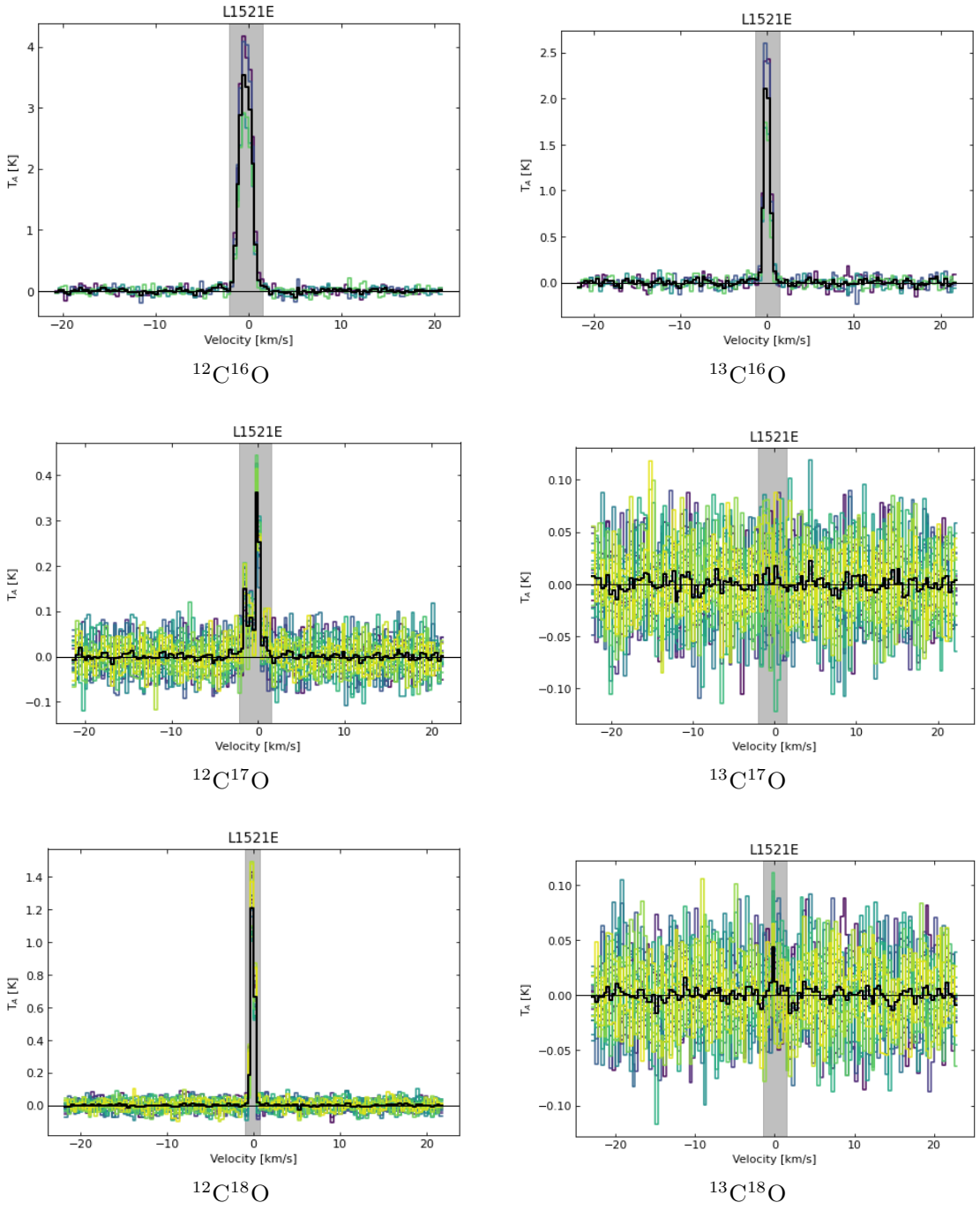

Figure 2. Spectra of the CO (2-1) rotational transition for the isotopologues in L1521E along with velocity masks over the stated velocity range in Table 2.

This lead to

$$\frac{\int T_{R,1} dv_1}{\int T_{R,2} dv_2} = \frac{N_1 \Delta v_1}{N_2 \Delta v_2}. \quad (4)$$

Equation 4 describes the relation between the ratio of integrated brightness temperature and the ratio of column densities. Lastly, we assumed that there is no chemical fractionation (Mangum & Shirley 2015). Thus, the ratio of column density is equal to the abundance ratio of two isotopes.

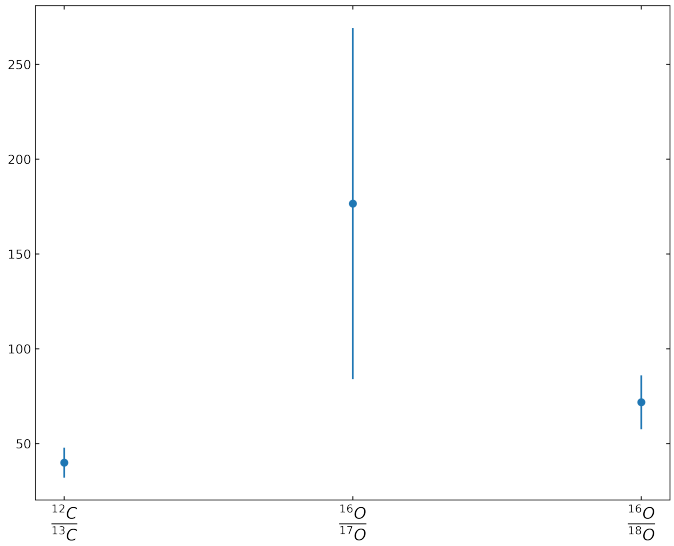

Figure 3. Isotopic abundance ratio in L1521E.

4. RESULTS

According to the derived Equation 4, we calculated the isotopic ratios of C and O from different line emission using their integrated temperature values and their velocity range, as stated in Table 2. Now, as stated in Section 3, due to our assumption of the lines having small optical depths, we ignore $^{12}C^{16}O$ line emission.

To calculate isotopic ratios of one element we kept the second element of the same species in our line ratios. We calculated the error using the propagation of error given the line ratios, integrated temperatures, and the respective errors on the integrated temperatures. Finally, we took the final result to be the one with the least error. The results for these isotopic ratios are shown in Table 3 and Figure 3.

Table 3. Calculated line ratios with uncertainties and final results of isotope abundance ratio in L1521E. The final abundance ratio is taken as the one with the least error.

Lines	Line Ratios	$\frac{^{12}C}{^{13}C}$	$\frac{^{16}O}{^{17}O}$	$\frac{^{16}O}{^{18}O}$
$^{12}C^{17}O/^{13}C^{17}O$	023.23 ±12.18			
$^{12}C^{18}O/^{13}C^{18}O$	039.95 ±07.89	39.95	176.57	71.81
$^{13}C^{16}O/^{13}C^{17}O$	176.57 ±92.57	±7.89	±92.57	±14.22
$^{13}C^{16}O/^{13}C^{17}O$	071.81 ±14.22			

5. SCIENTIFIC ANALYSIS AND DISCUSSION

Our calculated isotopic abundance ratios are around the known abundance ratios found for different starless clouds in the local interstellar medium (Langer & Penzias 1993). Our measured value of $\frac{^{12}C}{^{13}C}$ is lower than the observed value of 58.8 ± 3.7 stated in Ikeda et al. (2002). This might be the case of our poor signal-to-noise ratio of $^{13}C^{18}O$ line emission along with the assumptions and approximations taken in Section 3. The very large error in the observation of $\frac{^{16}O}{^{17}O}$ is due to very poor signal to noise ratio of $^{13}C^{17}O$ line emission.

The approximation taken in Section 3, namely that the line profile is rectangular, can be further modified to fit a Gaussian velocity profile. Langer & Penzias (1993)

shows the method of a weighted integrals, which would require a more precise line profile information. Thus, our future ambition is to estimate the most precise line profile for different lines.

6. CONCLUSION

We derived the isotopic abundance ratios, $\frac{^{12}C}{^{13}C}$, $\frac{^{16}O}{^{17}O}$, and $\frac{^{16}O}{^{18}O}$, in a starless cloud Lynds 1521E (L2521E), to be 39.95 ± 7.89, 176.57 ± 92.57, and 71.81 ± 14.22, respectively. These ratios can be made further precise by using a better data as to get the higher SNR for individual line emission. Furthermore, more precise calculation and information regarding properties such as line profiles would increase the precision of these ratios.

7. ACKNOWLEDGEMENT

The authors thank Dr. Daniel P. Marrone for supervising this project and guiding us through the finer details of radio observations.

REFERENCES

Ikeda, M., Hirota, T., & Yamamoto, S. 2002, ApJ, 575, 250, doi: 10.1086/341287

Langer, W. D., & Penzias, A. A. 1993, ApJ, 408, 539, doi: 10.1086/172611

Mangum, J. G., & Shirley, Y. L. 2015, PASP, 127, 266, doi: 10.1086/680323